Compressive Sensing–Based Reconstruction of Sea Free-Surface Elevation on a Vertical Wall

Valentina Laface[1]; Giovanni Malara[2]; Alessandra Romolo[3]; Felice Arena[4]; and Ioannis A. Kougioumtzoglou, M.ASCE[5]

Abstract: Measuring the free-surface displacement on a vertical wall of a marine structure is not a trivial problem. In this context, the efficacy of ultrasonic probes is affected by the interaction between the signal emitted by the sensor and the vertical wall, whereas image-based techniques are computationally demanding, especially if long-time series are utilized. Considering these difficulties, this paper proposes a novel approach for measuring the sea surface elevation on vertical breakwaters. The proposed methodology involves the use of pressure measurements and a reconstruction algorithm based on a compressive sensing (CS) technique in conjunction with a generalized harmonic wavelet (GHW) basis. In particular, a *constrained* CS optimization approach is proposed by utilizing the known values of the free-surface data to reconstruct all other missing data while adhering at the same time to prescribed upper and lower bounds at all time instants. The reliability of the methodology was assessed against field data pertaining to a vertical wall equipped with pressure transducers recorded at the Natural Ocean Engineering Laboratory of Reggio Calabria. It was shown that direct application of an unconstrained GHW-based CS optimization approach yielded physically inconsistent minima and maxima values; thus, it was inadequate for reliably reconstructing the free surface. These drawbacks were removed by the constrained GHW-based CS. Furthermore, examination of the reconstructed sea surface profiles in the vicinity of extremely high wave crests or wave troughs showed that they are in agreement with pertinent theoretical data obtained by using the nonlinear quasi-determinism theory. **DOI: 10.1061/(ASCE)WW.1943-5460.0000452.**

Author keywords: Compressive sensing; Vertical wall; Measurement; Constrained optimization; Extreme waves.

Introduction

Surface wave data are fundamental both for conducting experimental activities and for designing coastal and offshore installations, as well as for determining operational conditions of any structure/device deployed in the sea. However, direct measures of sea surface elevation in certain specific conditions may be difficult to achieve due to instrumentation limitations. For instance, ultrasonic wave gauges may be used for direct recording of sea surface elevation, but they often fail when measuring rough seas with strong wind and breaking waves. Furthermore, due to their working principle, they are not suitable for measuring waves close to or directly on structures. To overcome these limitations, one of the most common approaches is to derive indirectly the sea surface elevation by means of pressure measurements (Baquerizo and Losada 1995; Bishop and Donelan 1987; Deconinck et al. 2012; Kuo and Chiu 1994, 1995; Tsai et al. 2005; Tsai and Tsai 2009), or video image processing in the case of wave flume experiments (Lee and Kwon 2003; Viriyakijja and Chinnarasri 2015).

There are some advantages in utilizing subsurface sensors to measure surface waves. They do not need a supporting structure penetrating the sea surface and may be installed on the seabed to avoid damage by ships, fishing activities, and severe storms. The oldest and most widely used approach for deriving sea surface elevation from pressure measurements is the one based on Archimedes' relation using hydrostatic approximations (Dean and Dalrymple 1991; Kundu et al. 2015). Another approach is that of transfer function (TF), which is obtained by linearizing the equation of motion around the quiescent water level and by obtaining a linear relationship between the Fourier transform of the dynamic pressure and the sea surface elevation (Baquerizo and Losada 1995, Escher and Schlurmann 2008; Kundu et al. 2015; Kuo and Chiu 1994, 1995). Both methods are based on the linear wave theory and are not able to capture the nonlinear effects that are expected to be significant, for instance, in shallow waters. An improvement relates to the introduction of the nonlocal relationship approach for nonlinear sea surface reconstruction (Deconinck et al. 2012; Oliveras et al. 2012), whereas further enhancements of the classical TF approach include the renormalized transfer function (RTF) (Oliveras et al. 2012). Constantin (2012) developed a fully nonlinear explicit relation that may be applied for recovering sea surface elevation starting from the bottom pressure and the wave celerity. It is valid for solitary wave reconstruction only and is referred to as explicit solitary wave reconstruction (ESWR). An overview of the methodology relying on the determination of sea surface from pressure

[1]Post-Doc Research Fellow, Natural Ocean Engineering Laboratory (NOEL), "Mediterranea" Univ. of Reggio Calabria, Loc. Feo di Vito, Reggio Calabria 89122, Italy. Email: valentina.laface@unirc.it

[2]Post-Doc Research Fellow, Natural Ocean Engineering Laboratory (NOEL), "Mediterranea" Univ. of Reggio Calabria, Loc. Feo di Vito, Reggio Calabria 89122, Italy. Email: giovanni.malara@unirc.it

[3]Assistant Professor, Natural Ocean Engineering Laboratory (NOEL), "Mediterranea" Univ. of Reggio Calabria, Loc. Feo di Vito, Reggio Calabria 89122, Italy. Email: aromolo@unirc.it

[4]Professor, Natural Ocean Engineering Laboratory (NOEL), "Mediterranea" Univ. of Reggio Calabria, Loc. Feo di Vito, Reggio Calabria 89122, Italy (corresponding author). Email: arena@unirc.it, Tel. +39 09651692260.

[5]Assistant Professor, Dept. of Civil Engineering & Engineering Mechanics, Columbia Univ., New York, NY 10027. Email: ikougioum@columbia.edu

Note. This manuscript was submitted on June 22, 2017; approved on January 18, 2018; published online on June 18, 2018. Discussion period open until November 18, 2018; separate discussions must be submitted for individual papers. This paper is part of the ***Journal of Waterway, Port, Coastal, and Ocean Engineering***, © ASCE, ISSN 0733-950X.

measurements was given by Deconinck et al. (2012). To the best of the authors' knowledge, those approaches have never been applied for measuring the sea surface on a vertical wall despite its relevance in coastal engineering applications. Indeed, such a measurement allows, for instance, determining the crest height distribution, and thus characterizing a process with strongly nonlinear effects. In this context, the aforementioned theoretical tools appear inadequate for considering the reflected wave field in front of the structure. Therefore, this paper proposes an approach for reconstructing the free-surface elevation on a vertical wall by starting from pressure measurements recorded at various levels (above and below the mean sea level) on the structure and then processed via a harmonic wavelet based compressive sensing (CS) technique. CS (Candes and Wakin 2008; Donoho 2006) is a potent technique used in signal and image processing. The technique was proposed in the field of seismology (Claerbout and Muir 1973) and was recently revisited based on a robust mathematical foundation by Candes and Tao (2005, 2006) and Candes et al. (2006a, b). Indicative recent work on analyzing realizations of environmental (e.g., wind, earthquake, and sea wave) stochastic processes with limited data can be found in papers by Comerford et al. (2014, 2015, 2016, 2017) and Zhang et al. (2015, 2018). Specifically, it was demonstrated that the power spectral density function (either stationary or nonstationary) of the associated signals was recovered via CS even in cases of records with 85% missing data. Further applications in engineering dynamics include structural system parameter identification, damage detection, and health monitoring (Haile and Ghoshal 2012; Harley et al. 2012; Huang et al. 2014; Klis and Chatzi 2017; Kougioumtzoglou et al. 2017; Levine et al. 2012; Mascareñas et al. 2013; O'Connor et al. 2013; Perelli et al. 2015; Tau Siesakul et al. 2015; Wang and Hao 2015; Yang and Nagarajaiah 2015; Zou et al. 2015). The crux of the technique is the representation of a given signal in a certain basis by invoking the concepts of sparsity and incoherence. These properties allow utilizing highly sparse measurements and, subsequently, a relatively small number of data without the limits dictated by Shannon's theorem (Shannon 1949). Its potential for marine applications was further demonstrated recently by Laface et al. (2017), who showed that a CS technique allows for reliable reconstruction of sea surface elevation records even with a fraction of missing data greater than 60%.

Herein, the CS-based reconstruction of the free surface on a vertical wall is pursued and compared to a standard spline-based interpolation approach. Moreover, the signals reconstructed via harmonic wavelet based CS methodologies are compared to the nonlinear theoretical profile of the sea surface elevation given by the quasi-determinism theory (Boccotti 1981, 1983, 1989, 2014; Romolo and Arena 2013; Romolo et al. 2014). A further comparison is proposed by considering relevant numerical simulation results.

Reconstruction of Sea Surface Elevation on a Vertical Wall

This section describes the method for determining the time history of the sea surface elevation on a vertical seawall by utilizing pressure measurements. It involves two steps:

1. extrapolation of information about sea surface elevation at each time instant, and
2. reconstruction of the sea surface elevation via CS.

This last step is implemented via both a direct application of generalized harmonic wavelet (GHW)–based CS and a constrained GHW-based CS.

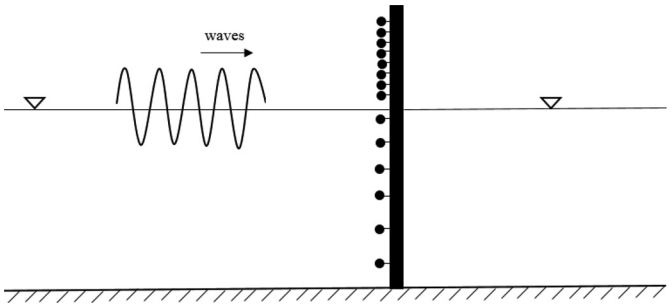

Fig. 1. Schematic of a vertical breakwater equipped with pressure transducers.

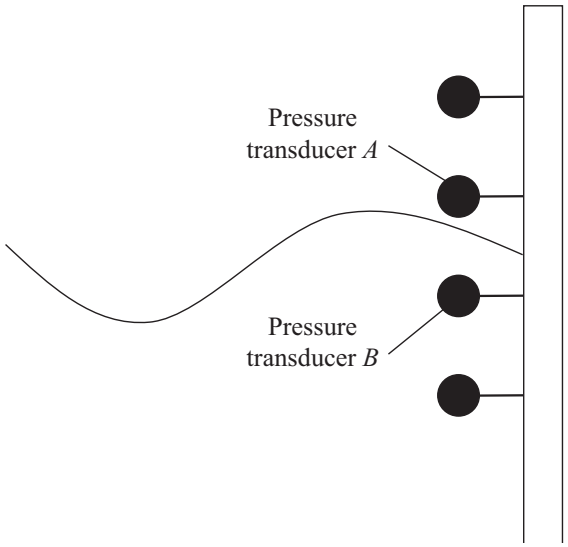

Fig. 2. Pressure Transducers A and B are the upper and lower bounds, respectively, of the instantaneous free-surface displacement on the vertical wall.

Information on the Instantaneous Free Surface from Pressure Measurements

Consider a vertical wall standing in a wave field and assume that the wall is equipped with pressure transducers located along a certain cross section (Fig. 1). This equipment is characterized by the fact that the transducers located under the free surface provide a measurement value different from zero, whereas the rest of the transducers provide null values. Overall, two types of information are obtained:

1. upper and lower bounds of the location of the instantaneous free surface, and
2. values of the instantaneous free surface at specific time instants.

The first type of information is obtained by analyzing two contiguous transducers, say A and B, characterized by the fact that A provides a null value and B provides a measurement different from zero at a certain time instant. In this context, the level of B is a lower bound, whereas the level of A is an upper bound (Fig. 2). The second type of information is obtained by identifying two consecutive samples recorded by a certain pressure transducer characterized by the fact that one sample provides a null value, whereas the other one provides a measurement. This condition occurs when the free surface is crossing the sensor level. Therefore, it is an indirect measure of the instantaneous free-surface level (Fig. 3). Obviously, the

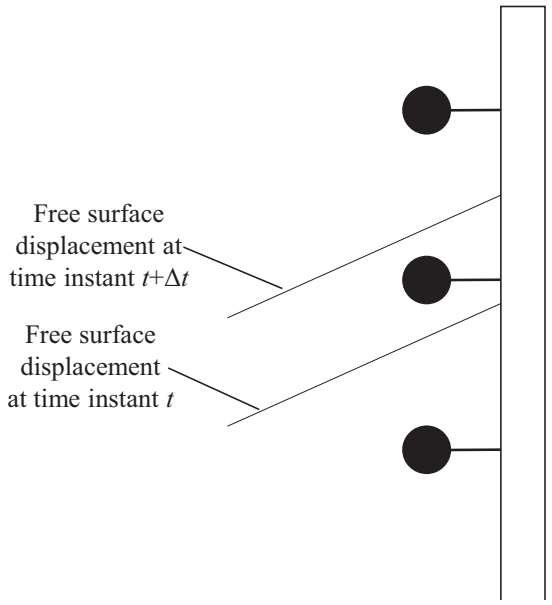

Fig. 3. Free surface level is under the central pressure transducer at time t, whereas it is above it at time $t + \Delta t$. Therefore, the free-surface level between these time instants is equal to the sensor level.

precise time instant associated with the sensor crossing cannot be identified. However, the error in its identification is of the same order of the sampling time.

Once the information on the surface elevation level at each time instant is determined, two different approaches can be adopted for reconstructing the sea surface elevation. The first is to process only the time instants at which the free-surface displacement is known. In this context, the information concerning the upper and lower bounds is not invoked. Thus, the rest of the free-surface data are regarded as missing data, and the free-surface time history is processed by the standard GHW-based CS technique (Comerford et al. 2014, 2016). The second approach is to formulate a constrained optimization problem by enforcing the CS technique to include the information about the upper and lower bounds as well. These methods are described in the next subsections.

GHW-Based CS

CS is a recently developed technique used in signal and image processing and has been shown to be quite effective for reconstructing signals even in cases of missing data (Comerford et al. 2016).

The method consists of expanding the recorded signal in a given basis where the signal is sparse and in determining the expansion coefficients by solving a system of linear equations

$$y = Ax \tag{1}$$

where A = so-called sampling matrix; y = measurement vector containing the values of the recorded signal; and x = vector of the expansion coefficients to be determined. Regarding missing data, let N_0 be the original sample size and N_m the number of missing data, A is a $(N_0 - N_m)$ by N_0 matrix, whereas y and x have lengths $(N_0 - N_m)$ and N_0, respectively. In this regard, the system of linear equations given by Eq. (1) is underdetermined, and a sparse solution of x is obtained by an L_p–norm $(0 < p \le 1)$ minimization procedure (Comerford et al. 2014, 2016; Zhang et al. 2018).

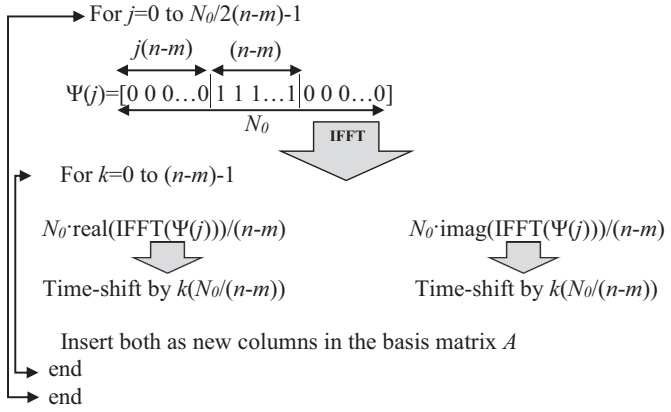

Fig. 4. Sampling matrix construction with GHW basis. IFFT denotes the Inverse Fast Fourier Transform.

The technique requires that both the signal and the sampling matrix satisfy certain properties (Candes and Wakin 2008). Specifically, the signal must be sparse in the selected basis. That is, it can be represented by a number of coefficients smaller than that determined at the Shannon-Nyquist rate (Nyquist 1928; Shannon 1949). Furthermore, the sampling and transformation domains must have high incoherence, which implies a nonsparse representation of the signal in the sampling domain. In addition to signal sparsity and incoherence, the sampling matrix must satisfy the restricted isometry property (RIP), which implies that if the signal has sparsity K (i.e., it can be represented by K nonzero coefficients), any matrix obtained by K randomly selected columns of A should have full rank and be nearly orthonormal. The implementation of the CS technique requires two main steps:

- construction of the sampling matrix (A), and
- L_p–norm $(0 < p \le 1)$ minimization procedure for determining x.

To construct the sampling matrix (A), an appropriate basis has to be selected. Herein, the GHW was considered, which is expressed in the frequency domain as (Newland 1994)

$$\Psi_{(m,n),k}(\omega) = \begin{cases} \dfrac{1}{(n-m)\Delta\omega} e^{-\dfrac{i\omega k T_0}{n-m}}; & m\Delta\omega \le \omega < n\Delta\omega \\ 0; & \text{elsewhere} \end{cases} \tag{2}$$

where T_0 = total time duration of the signal under consideration; m and n = integer numbers defining the frequency band; and $\Delta\omega = 2\pi/T_0$. The complex harmonic wavelet coefficients are given by

$$\left[W^G_{(m,n),k} f(t) \right] = \frac{(n-m)}{T_0} \int_{-\infty}^{+\infty} f(t) \Psi^*_{(m,n),k}(t) dt \tag{3}$$

Once the basis has been selected, a full N_0 by N_0 sampling matrix is generated by implementing the algorithm in Fig. 4. The GHW bases are generated by inverse fast Fourier transform, and then each of them is shifted $(n - m)$ times in the time domain to form an orthogonal basis. When the construction of A is completed, N_m rows corresponding to the position of the missing data are removed and the system of linear equations [Eq. (1)] is solved by an L_p–norm $(0 < p \le 1)$ minimization procedure. Finally, the reconstructed signal is obtained by multiplying the full N_0 by N_0 sampling matrix by the solution x.

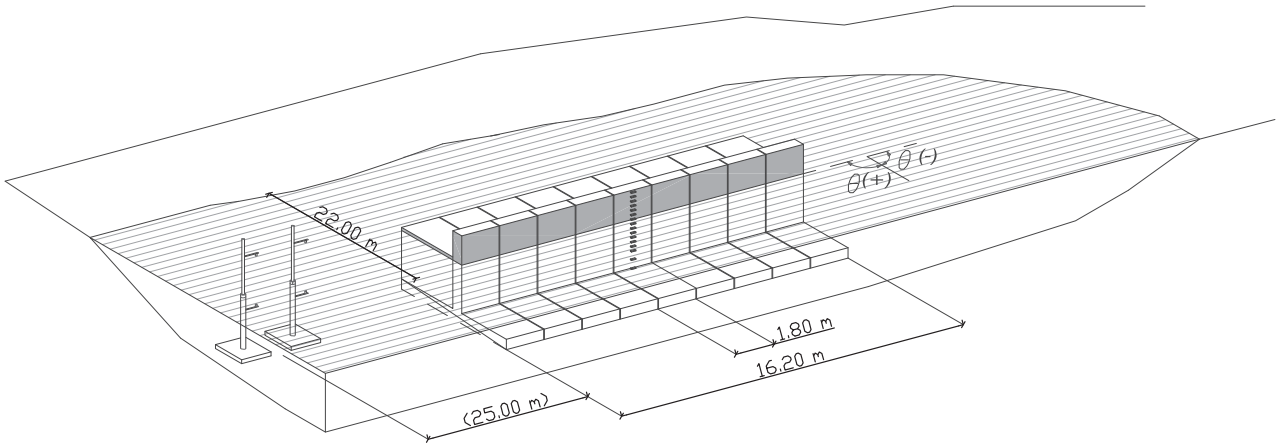

Fig. 5. Experimental layout: small-scale model of the breakwater and location of the vertical piles in the undisturbed wave field.

Constrained GHW-Based CS

In the "GHW-Based CS" section, additional available information relating to upper and lower bounds of the sea surface was not utilized in the reconstruction methodology. Therefore, in this section, it is proposed to take into account both the known values of the free surface and the upper/lower bounds of the free surface in the problem formulation. Specifically, the equality constraint given by Eq. (1) is considered for the N_{eq} time instants at which the exact values of the sea surface are identified. For the remaining N_{in} time instants, the fact that the sea surface level is confined within a given range is expressed by an inequality of the form

$$y_{\inf} \leq A_{in}x \leq y_{\sup} \tag{4}$$

where $A_{in} = N_{in}$ by N_0 matrix obtained from the full N_0 by N_0 sampling matrix by removing the rows associated with the N_{eq} known values of the free surface; and $y_{\inf}$ and $y_{\sup}$ = vectors of length N_{in} providing the lower and upper bounds, respectively. Thus, such a problem constitutes a constrained optimization problem of the form

$$\min_x l_1 \quad \text{such that} \begin{cases} Ax = y \\ y_{\inf} \leq A_{in}x \leq y_{\sup} \end{cases} \tag{5}$$

which can be solved by trust-region-reflective or interior-point algorithms (Byrd et al. 2000; Waltz et al. 2006). For this purpose, the objective function minimized by the algorithm is the l_1 norm of x. The procedure is initiated by starting from the solution x_0 obtained by the standard harmonic wavelet based CS as described in the "GHW-Based CS" section.

Results

This section discusses a data analysis concerning the reconstruction of the free-surface displacement from pressure measurements. The input data were field data collected at the natural basin of the Natural Ocean Engineering Laboratory (NOEL) of Reggio Calabria (Italy). First, the layout of the experiment is described. Next, the numerical results are discussed. In this context, the proposed CS procedure is compared with a simple cubic spline–based interpolation for highlighting the limitations associated with standard interpolation schemes.

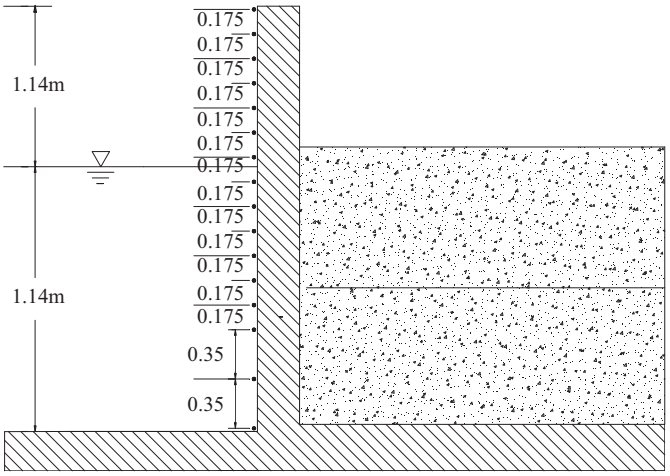

Fig. 6. Cross section of the breakwater equipped with pressure transducers.

Experimental Setup

The NOEL laboratory is a natural test site with wind conditions generating sea states of pure wind waves that are small-scale models in a Froude similarity of ocean sea states. The data collected during an experiment conducted on a small-scale model of a vertical breakwater were utilized herein for assessing the reliability of the proposed technique. The experimental setup was described by Boccotti et al. (2012), who ran the experiment to analyze wave forces and pressure distributions on the vertical wall. The breakwater utilized in the experiment had a height of 3 m, a length of 16.2 m, and was installed on a water depth of approximately 1.9 m (Fig. 5). In this regard, note that the tidal variation was within ± 0.15 m.

The midsection of the breakwater was equipped with pressure transducers located on a vertical bar. Specifically, 16 sensors were placed below and above the mean water level. In this regard, considering the fact that free-surface oscillations are supposed to occur mainly around the mean water level, the distance between the sensors was kept minimal near the mean water level and slightly larger near the sea bottom, as shown in the schematic in Fig. 6. Fig. 5 also shows two piles located 25 m from the breakwater. The piles were equipped with a pair of ultrasonic probes and were used for recording the incident wave field. Each recorded sea state was sampled at

10 Hz over a 5-min time span. Thus, each record was composed of 3,000 samples per sensor.

Two sea states were analyzed in the next subsection. The first sea state had a peak spectral period of 2.21 s, a mean spectral period of 1.63 s, a dominant wavelength of 7.7 m, and a dominant direction of 8° (where 0° means waves orthogonal to the breakwater). The second one was characterized by a peak period of 2.37 s, a mean period of 1.53 s, a dominant wavelength of 8.3 s, and a dominant direction of 3°. Thus, the ratio between the breakwater length and the wavelength was approximately equal to 2, so that the pressure measurements were considered representative of a fully reflected wave field. These records were chosen because one possessed a very high crest and the other one, a very deep trough. Thus, they allowed testing the proposed methods in conjunction with severe events. Finally, note that the wave reconstruction in the numerical examples refers to the time domain only (as opposed to the joint time-space domains), and thus, the effect of wave angle is irrelevant.

Data Analysis

The exact values of the free-surface elevation were extrapolated from pressure measurements via the procedure described in the "Reconstruction of Sea Surface Elevation on a Vertical Wall" section. Next, the reconstruction was pursued first by interpolating the data via a cubic spline scheme (Fig. 7). Specifically, *MATLAB*'s spline function was used (de Boor 1978), which involved the solution of a tridiagonal linear system of equations for determining the coefficients of the involved cubic polynomials in the interpolating spline. Fig. 7(a) shows the full reconstruction for a time window of 50 s, during which both large- and small-amplitude waves occurred. It is seen that the spline interpolation rendered a good approximation of the wave profile in the proximity of the larger-amplitude waves, but it was not capable of capturing the oscillatory nature of smaller-amplitude waves as it led to a flat signal. This problem was observed at 10 and 20 s, and relates to the fact that the free surface oscillated around the level of one transducer only. Therefore, a standard interpolation scheme was inadequate to handle this practical problem. Furthermore, if one or more sensors experienced a failure, this problem may be significantly more evident. In this regard, an example is shown in Fig. 7(b), where the dashed line represents the level of the sensor that was not working. Comparing Figs. 7(a and b), it can be easily noticed that if just one sensor fails, the number of known values of the free surface decreases significantly, and the performance of the spline interpolation becomes even worse, leading to additional flat regions at 35 and 45 s. For these reasons, more sophisticated mathematical tools are needed. Specifically, a reconstruction method working efficiently even with a relatively large percentage of missing data is required. For this purpose, the GHW-based CS technique was considered herein, which has already been applied efficiently for reconstructing records of sea surface elevation in an undisturbed wave field with more than 60% of missing data (Laface et al. 2017).

Next, for each record, the analysis considered a time window of few tens of seconds in the vicinity of the largest-amplitude wave. The data were processed by following the procedure described in the "Information on the Instantaneous Free Surface from Pressure Measurements" section to identify the exact values of the sea surface elevation and its range of variability at the time instants when

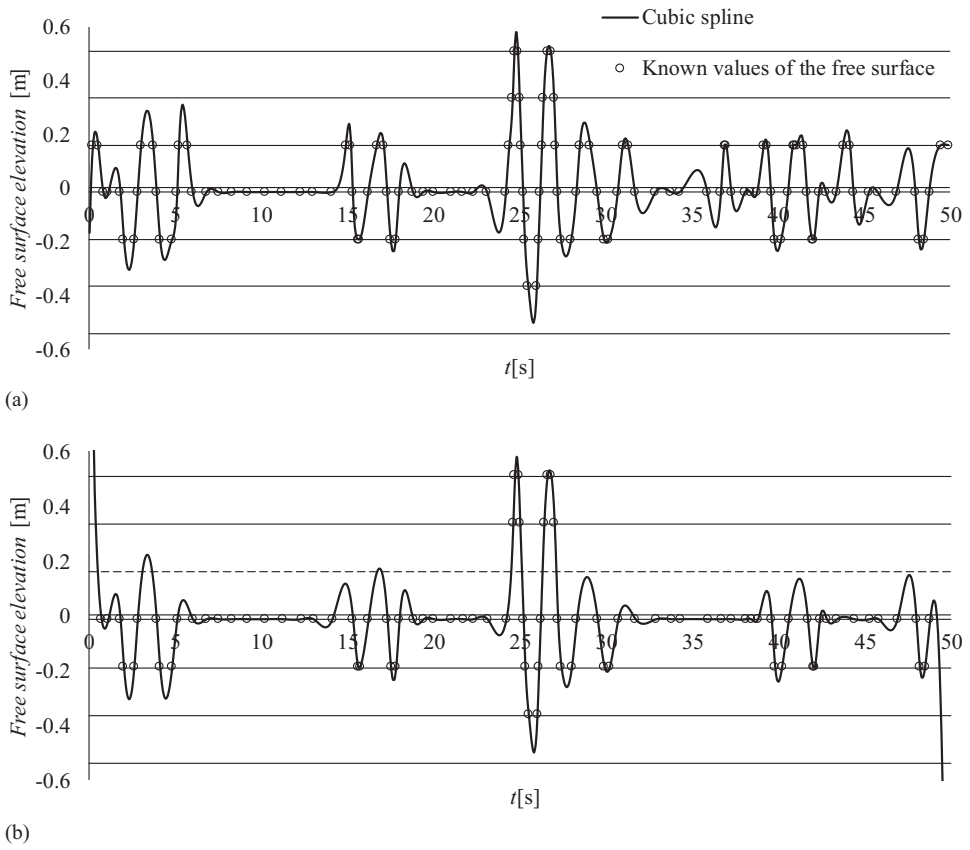

Fig. 7. Free surface elevation reconstructed by a cubic spline. The horizontal lines denote the sensor levels: (a) interpolation conducted by using all sensors; and (b) interpolation conducted by simulating the failure of one sensor (denoted by the dashed line).

J. Waterway, Port, Coastal, Ocean Eng., 2018, 144(5): 04018010

no exact information was available. Next, the sea surface was reconstructed via two different approaches:

- classical GHW-based CS technique in the case of missing data (see the "GHW-Based CS" section) and a l_1 norm minimization, and
- constrained GHW-based CS technique (see the "Constrained GHW-Based CS" section).

A direct measurement of the free-surface displacement was not available. Therefore, to test the effectiveness of the proposed methodology, the reconstructed sea surface elevations were compared with that obtained by means of the second-order solution given by the quasi-determinism theory presented by Romolo and Arena (2013) (see the appendix for a concise description of the theory). In addition, a comparison with relevant results from numerical simulations is proposed, as it allows straightforwardly comparing the reconstructed free surface to a target (known) simulated free-surface elevation.

The quasi-determinism theory is used for describing the free surface in the vicinity of the highest wave of the record. The comparison between the reconstructed and theoretical sea surface elevations is given in Figs. 8 and 9 for the cases of high crest and deep trough, respectively. It is seen that, in both cases, the reconstruction pursued via standard GHW-based CS led to a signal with considerable level of noise. Furthermore, the reconstruction was characterized by physically inconsistent local minima between two consecutive samples having the same (known) levels. Similar considerations held for the reconstruction of the trough as well.

The two problems encountered in the reconstruction via standard GHW-based CS were overcome via the constrained GHW-based CS. Indeed, the reconstruction was not affected by unexpected local maxima/minima. In this context, a comparison with the nonlinear quasi-determinism (QD) theory showed that there was a good agreement between reconstructed and theoretical sea surface elevations in the vicinity of the largest-amplitude wave.

Finally, the proposed technique was compared to the spline-based interpolation. The results are shown in Fig. 10, which considers the cases of both fully operative sensors and one failed sensor. It is shown that this methodology clearly reproduced the salient

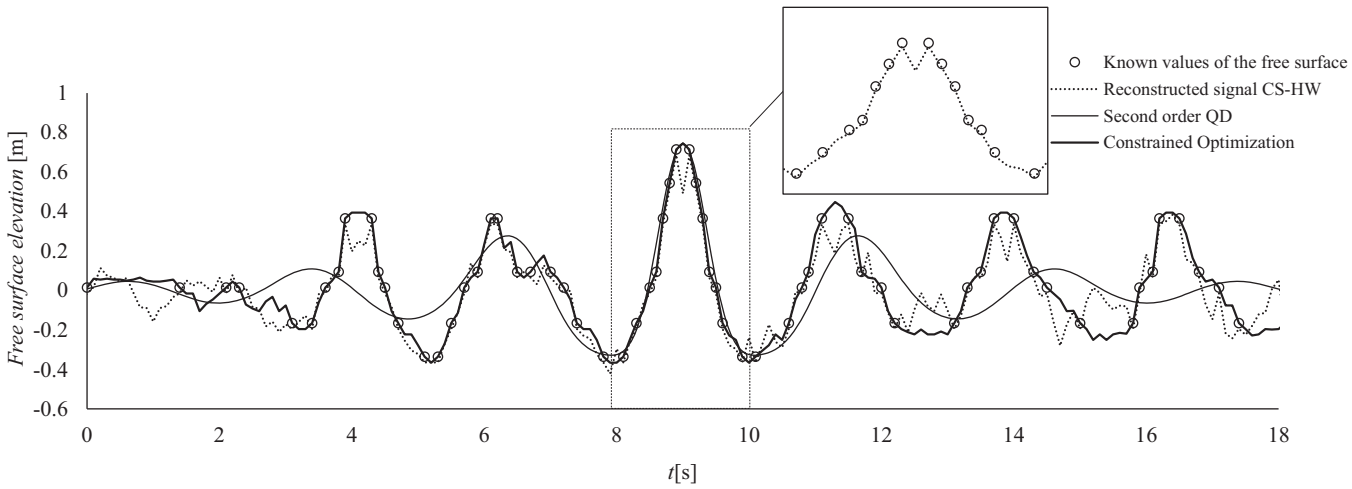

Fig. 8. Comparison between reconstructed and theoretical free-surface elevations in the vicinity of an extremely high wave crest. The small windows show that the classical reconstruction by CS may lead to physically inconsistent local minima in the highest wave. QD = quasi-determinism; HW = harmonic wavelet.

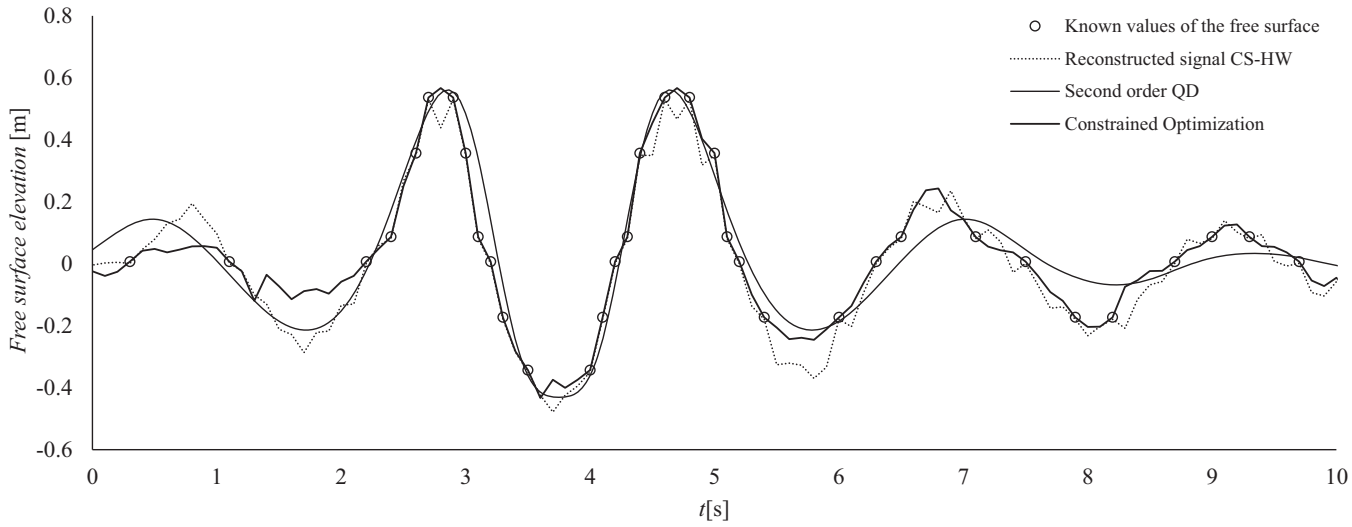

Fig. 9. Comparison between reconstructed and theoretical free-surface elevations in the vicinity of an extremely deep wave trough. QD = quasi-determinism; HW = harmonic wavelet.

J. Waterway, Port, Coastal, Ocean Eng., 2018, 144(5): 04018010

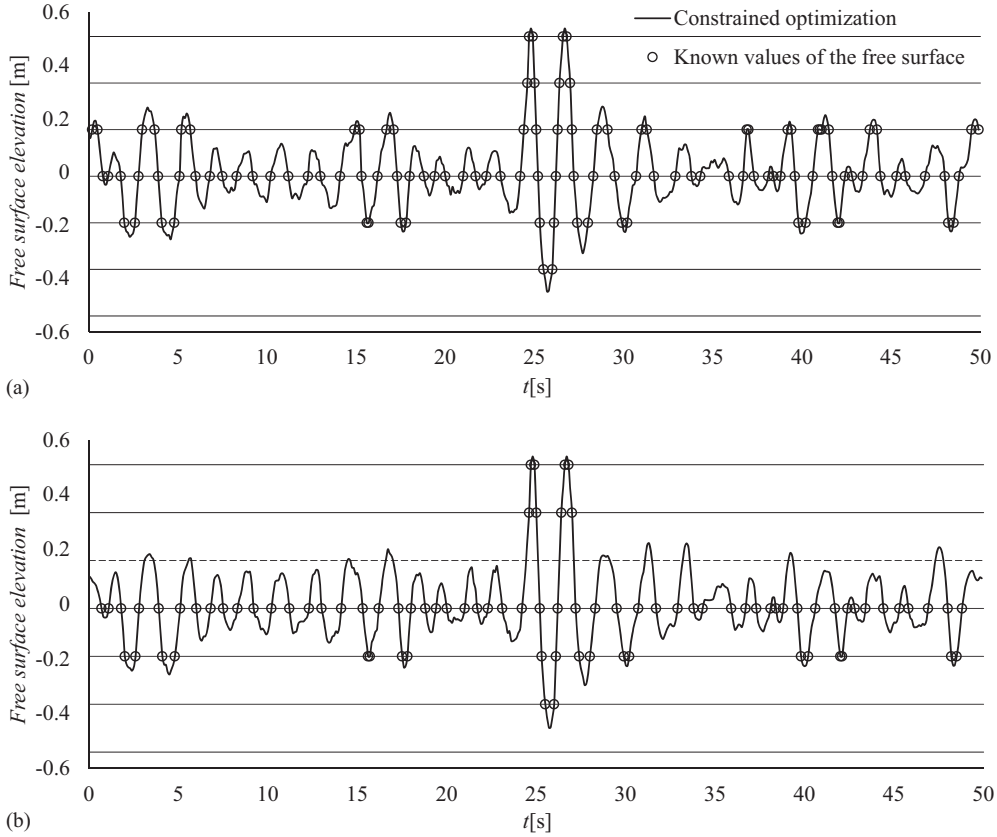

Fig. 10. Free surface elevation reconstructed via constrained GHW-based CS: (a) reconstruction conducted by using all sensor data; and (b) reconstruction conducted by assuming the failure of one sensor (denoted by a dashed line).

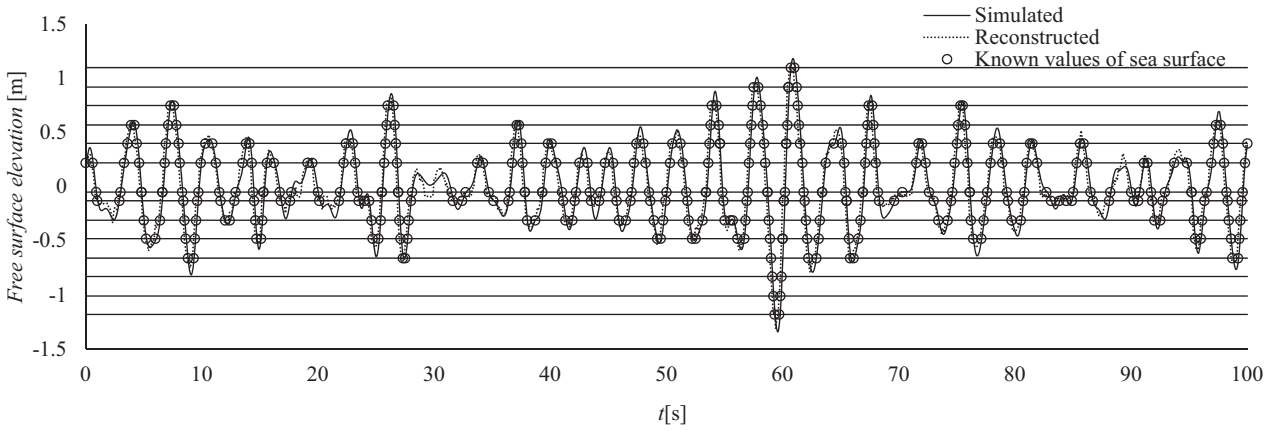

Fig. 11. Comparison between the free-surface elevation obtained by the numerical simulation (continuous line) and the reconstructed free surface obtained by the constrained GHW-based CS.

features of the wave profile and overcame the aforementioned problems (e.g., flat regions) associated with the standard interpolation schemes, such as splines.

A further test of the proposed methodology was pursued by comparing the result of the reconstruction with a numerical simulation of the free-surface elevation at the seawall. A 5-min realization of the free-surface elevation was synthesized under the assumption that the underlying sea state was compatible with a mean Joint North Sea Wave Project (JONSWAP) frequency spectrum (Hasselmann et al. 1973) having a peak frequency of 1.9 rad/s and significant wave height of 0.6 m. Then, the known values and the interval of possible values of the free surface were identified a posteriori to simulate the operation of given pressure transducers located on the wall. Such a procedure provided the input data to the constrained CS algorithm that was thus utilized for reconstructing the free-surface elevation. The result is shown in Fig. 11 for a time window of 100 s in conjunction with the known values of the free surface and the pressure transducer levels. Even in this case, it is seen that the reconstructed signal was in quite good agreement with the simulated one.

Concluding Remarks

In this paper, a method was developed for measuring the sea surface elevation directly on a vertical breakwater. A new approach was proposed, which consists of predicting sea surface elevation values by utilizing pressure measurements recorded at different levels along the vertical wall. The proposed method determines, for certain time instants, the exact values of the sea surface elevation through the identification of pressure transducer crossings and, for the remaining time instants, the range of variability. Then, these data are used as input for a full reconstruction of the sea surface elevation via two distinct approaches: standard GHW-based CS and constrained GHW-based CS. The reconstructed sea surface obtained via the reconstruction methods mentioned earlier was compared to the numerical results obtained by means of the nonlinear (second-order) quasi-determinism theory. Results showed that the standard GHW-based CS reconstructed a free-surface profile characterized by a considerable noise level and by inconsistent local minima and maxima in the time domain. These limitations were overcome by the constrained GHW-based CS reconstruction, which rendered the free-surface profile consistent with the information provided by the pressure measurements and in agreement with the QD profile in the vicinity of the extreme crest/trough. Furthermore, comparisons with a standard spline-based interpolation scheme demonstrated the inadequacy of the splines to capture salient features of the wave profiles, and justified the utilization of more sophisticated methodologies, such as the herein-proposed CS-based one.

Appendix. Nonlinear Quasi-Determinism Theory for Standing Wave Groups

The quasi-determinism theory was proposed in the 1980s for describing the evolution of sea waves in the vicinity of extremely high crests, troughs, or crest-to-trough wave heights. Its physical interpretation as well as its implementation in conjunction with marine-related problems was pursued by Boccotti (1982, 1983, 1989), and experimental validations through laboratory and satellite data were proposed in the 1990s (Boccotti et al. 1993; Phillips et al. 1993a, b). The fundamental result of the theory is that, when an extremely high wave crest of given height H_c occurs at a certain point $\underline{x}_0 \equiv (x_0, y_0)$ at time instant t_0 in a random stationary Gaussian wind-generated sea state, the free-surface elevation near the extreme wave is well approximated by the deterministic equation

$$\overline{\eta}(\underline{x}_0 + \underline{X}, t_0 + T) = H_C \frac{\Psi(\underline{X}, T)}{\Psi(\underline{0}, 0)} \tag{6}$$

where Ψ = autocovariance of the free-surface displacement process in which the exceptionally high crest elevation occurs, and it is defined as

$$\Psi(\underline{X}, T) = < \eta(\underline{x}_0, t)\, \eta(\underline{x}_0 + \underline{X}, t + T) > \tag{7}$$

The main properties of the theory are that it can be applied to a nearly arbitrary bandwidth of the spectrum, and to sea waves propagating either in an undisturbed wave field or in a diffracted wave field. Therefore, it can be used for calculating the free-surface elevation in front of a vertical seawall. The basic assumption of this theory is that the wave crest (H_C) of the free-surface elevation has to be exceptionally high with respect to the root-mean square surface displacement (σ) of the random wave field where it occurs. Experimental data have shown that an excellent agreement between the theoretical profiles and the recorded data is reached for ratios of $H_C/\sigma > 3.5$.

Recently, the theory was further developed by Romolo and Arena (2013) for sea wave groups interacting with a reflective breakwater including second-order nonlinear effects. The approximation of the free-surface displacement derived by them and utilized in this paper is the following:

$$\overline{\eta}(\underline{x}_0 + \underline{X}, t_0 + T) = \overline{\eta}_{R_1}(\underline{x}_0 + \underline{X}, t_0 + T) + \overline{\eta}_{R_2}(\underline{x}_0 + \underline{X}, t_0 + T) \tag{8}$$

where

$$\overline{\eta}_{R_1}(\underline{x}_0 + \underline{X}, t_0 + T) = 4 \frac{H_C}{\sigma_R^2} \int_0^{\infty} \int_0^{2\pi} S(\omega, \theta) \cos(kX \sin\theta - \omega T) \times \cos(k y_0 \cos\theta) \cos[k(y_0 + Y) \times \cos\theta] d\theta\, d\omega \tag{9}$$

$$\begin{aligned}\overline{\eta}_{R_2}(\underline{x}_0 + \underline{X}, t_0 + T) = \frac{2H_C^2}{\sigma_R^4} \int_0^{\infty} \int_0^{\infty} \int_0^{2\pi} \int_0^{2\pi} S(\omega_1, \theta_1) S(\omega_2, \theta_2) \cos(\phi_1) \\ \times \cos(\phi_2) \Big\{ \left[A_1^- \cos(\alpha_1 - \alpha_2) \right. \\ \left. + A_2^- \cos(\alpha_1 + \alpha_2) \right] \cdot \cos(\lambda_1 - \lambda_2) \\ + \left[A_1^+ \cos(\alpha_1 + \alpha_2) + A_2^+ \cos(\alpha_1 - \alpha_2) \right] \\ \times \cos(\lambda_1 + \lambda_2) \Big\} d\theta_2\, d\theta_1\, d\omega_2\, d\omega_1 - (\Xi/g)\end{aligned} \tag{10}$$

$$\sigma_R^2 = \sigma_R^2(y_0) = 4 \int_0^{\infty} \int_0^{2\pi} S(\omega, \theta) \cos^2(k y_0 \cos\theta) d\theta\, d\omega \tag{11}$$

where g = acceleration due to gravity; $S(\omega, \theta)$ = directional wave spectrum of the incident waves; and the wave frequency (ω) and wave number (k) are related by the linear dispersion rule

$$\omega^2 = gk \tanh(kd) \tag{12}$$

$S(\omega_n, \theta_n)$ ($n = 1, 2$) = directional wave spectrum of the incident waves; and ϕ_n, α_n, and λ_n, ($n = 1, 2$) are defined by relations

$$\begin{aligned}&\phi_n(k_n, \theta_n, y_0) = k_n y_0 \cos\theta_n \\ &\alpha_n(k_n, \theta_n, y_0, Y) = k_n \cos\theta_n (y_0 + Y), \text{ for } n = 1, 2 \\ &\lambda_n(k_n, \theta_n, X, T) = k_n \sin\theta_n X - \omega_n T\end{aligned} \tag{13}$$

and the coefficients $A_n^{\mp}$ ($n = 1, 2$) = interaction kernels of the nonlinear surface displacement, which are defined as

$$\begin{aligned}A_n^-(\omega_1, \omega_2, \theta_1, \theta_2) = g^{-1} D_n^- + g\omega_1^{-1}\omega_2^{-1} B_n^- \\ A_n^+(\omega_1, \omega_2, \theta_1, \theta_2) = g^{-1} D_n^+ + g\omega_1^{-1}\omega_2^{-1} B_n^+\end{aligned}, \text{ for } n = 1, 2 \tag{14}$$

with coefficients $D_n^{\mp}$ ($n = 1, 2$) expressed by

$$D_n^-(\omega_1,\omega_2,\theta_1,\theta_2)=(-1)^n\frac{g^2k_1k_2}{\omega_1\omega_2}\cos\left[\theta_1+(-1)^n\theta_2\right]+(\omega_1+\omega_2)^2-3\omega_1\omega_2$$
$$D_n^+(\omega_1,\omega_2,\theta_1,\theta_2)=(-1)^n\frac{g^2k_1k_2}{\omega_1\omega_2}\cos\left[\theta_1+(-1)^n\theta_2\right]+(\omega_1+\omega_2)^2-\omega_1\omega_2 \quad \text{, for } n=1,\,2 \tag{15}$$

In Eq. (14) the coefficients $B_n^{\mp}$ ($n = 1, 2$) are given by

$$B_n^-(\omega_1,\omega_2,\theta_1,\theta_2)=-\frac{\Lambda_n^-\omega_1\omega_2(\omega_1-\omega_2)/g^2}{(\omega_1-\omega_2)^2-g|\underline{\mathbf{k}}_n^-|\tanh\left(|\underline{\mathbf{k}}_n^+|d\right)}$$
$$B_n^+(\omega_1,\omega_2,\theta_1,\theta_2)=-\frac{\Lambda_n^+\omega_1\omega_2(\omega_1+\omega_2)/g^2}{(\omega_1+\omega_2)^2-g|\underline{\mathbf{k}}_n^+|\tanh\left(|\underline{\mathbf{k}}_n^+|d\right)} \quad \text{, for } n=1,\,2 \tag{16}$$

with

$$\begin{aligned}\Lambda_n^-(\omega_1,\omega_2,\theta_1,\theta_2)=&-\frac{\omega_1^3}{\sinh^2(k_1d)}+\frac{\omega_2^3}{\sinh^2(k_2d)}-2\omega_1\omega_2(\omega_1-\omega_2)\\&-(-1)^n2g^2\left(\omega_1^{-1}-\omega_2^{-1}\right)k_1k_2\cos\left[\theta_1+(-1)^n\theta_2\right]\\ \Lambda_n^+(\omega_1,\omega_2,\theta_1,\theta_2)=&-\frac{\omega_1^3}{\sinh^2(k_1d)}-\frac{\omega_2^3}{\sinh^2(k_2d)}+2\omega_1\omega_2(\omega_1+\omega_2)\\&+(-1)^n2g^2\left(\omega_1^{-1}+\omega_2^{-1}\right)k_1k_2\cos\left[\theta_1+(-1)^n\theta_2\right]\end{aligned} \quad \text{, for } n=1,\,2 \tag{17}$$

and

$$\underline{\mathbf{k}}_n^-(\omega_1,\omega_2,\theta_1,\theta_2)=\left(k_1\sin\theta_1-k_2\sin\theta_2;\ k_1\cos\theta_1+(-1)^nk_2\cos\theta_2\right)$$
$$\underline{\mathbf{k}}_n^+(\omega_1,\omega_2,\theta_1,\theta_2)=\left(k_1\sin\theta_1+k_2\sin\theta_2;\ k_1\cos\theta_1-(-1)^nk_2\cos\theta_2\right), \quad \text{for } n=1,\,2 \tag{18}$$

Finally, the constant Ξ in Eq. (10) is given by the following relation:

$$\Xi=-g\frac{2H_C^2}{\sigma_R^4}\int_0^{\infty}\int_0^{\infty}\int_0^{2\pi}\int_0^{2\pi}S(\omega_1,\theta_1)S(\omega_2,\theta_2)F(\omega_1,\omega_2,\theta_1,\theta_2)d\theta_2\,d\theta_1\,d\omega_2\,d\omega_1 \tag{19}$$

being

$$F(\omega_1,\omega_2,\theta_1,\theta_2)=\begin{cases}\dfrac{2k_1}{\sinh(2k_1d)}\cos^2(\phi_1) & \text{if } \omega_1=\omega_2 \text{ and } \theta_1=\theta_2\\ 0 & \text{if } \omega_1\neq\omega_2 \text{ and } \theta_1\neq\theta_2\end{cases} \tag{20}$$

Eqs. (9) and (10) refer to a frame of reference in which an absolute Cartesian coordinate system $(\underline{x}, z) = (x, y, z)$ with origin on the mean water level is such that the breakwater is placed on the plane $y = 0$, where x represents the second (transversal) horizontal direction, and z is the vertical direction, positive upward. θ is the angle between the y-axis and the direction of the wave propagation, which is 0 for orthogonal waves.

The input data required for estimating the free-surface time history are the directional spectrum [$S(\omega, \theta)$] and the linear crest height (H_c) [in Eqs. (9) and (10)]. Furthermore, the location $(\underline{x}_0) \equiv (x_0, y_0)$ where the highest wave crest occurs must be specified by introducing an auxiliary Cartesian coordinate system, $(\underline{X}, z) = (X, Y, z)$, such that $\underline{x} = \underline{x}_0 + \underline{X}$.

In this paper, the directional spectrum $S(\omega,\theta)$ was calculated by applying the technique proposed by Boccotti et al. (2011) by considering the measurements of the gauges located on two piles in an undisturbed field (shown in Fig. 5) far from the breakwater. The linear crest height (H_c), occurring on the breakwater at the point $(\underline{x}_0) = \underline{0}$, was calculated by enforcing the equality between the absolute maximum of the reconstructed free-surface elevation and the maximum of the nonlinear $\overline{\eta}$ [Eq. (8)], so that the ratio between the highest crest height and the standard deviation of the reconstructed surface elevation was equal to 3.7 and 4.0 for the records of Figs. 8 and 9, respectively. The corresponding values of H_c/σ were assumed equal to 3.1 for the case of Fig. 8 and 3.5 for that of Fig. 9.

Acknowledgments

This paper was developed during the Marie Curie IRSES project "Large Multi Purpose Platforms for Exploiting Renewable

Energy in Open Seas (PLENOSE)" funded by the European Union (Grant Agreement Number PIRSES-GA-2013–612581). I. A. Kougioumtzoglou gratefully acknowledges the support by the Civil, Mechanical, and Manufacturing Innovation (CMMI) Division of the National Science Foundation, USA (Award Number 1724930).

References

Baquerizo, A., and M. A. Losada. 1995. "Transfer function between wave height and wave pressure for progressive waves, by Y.-Y. Kuo and J.-F. Chiu: Comments." *Coastal Eng.* 24 (3): 351–353. https://doi.org/10.1016/0378-3839(94)00038-Y.

Bishop, C. T., and M. A. Donelan. 1987. "Measuring waves with pressure transducers." *Coastal Eng.* 11 (4): 309–328. https://doi.org/10.1016/0378-3839(87)90031-7.

Boccotti, P. 1981. "On the highest waves in a stationary Gaussian process." *Atti Acc. Ligure di Scienze e Lettere.* 38: 271–302.

Boccotti, P. 1982. "On ocean waves with high crests." *Meccanica.* 17 (1): 16–19. https://doi.org/10.1007/BF02156003.

Boccotti, P. 1983. "Some new results on statistical properties of wind waves." *Appl. Ocean Res.* 5 (3): 134–140. https://doi.org/10.1016/0141-1187(83)90067-6.

Boccotti, P. 1989. "Quasi-determinism of sea wave groups." *Meccanica.* 24 (1): 3–14. https://doi.org/10.1007/BF01575998.

Boccotti, P. 2014. *Wave mechanics and wave loads on marine structures, butterworth.* Oxford: Butterworth-Heinemann.

Boccotti, P., F. Arena, V. Fiamma, A. Romolo, and G. Barbaro. 2011. "Estimation of mean spectral directions in random seas." *Ocean Eng.* 38 (2–3): 509–518. https://doi.org/10.1016/j.oceaneng.2010.11.018.

Boccotti, P., F. Arena, V. Fiamma, A. Romolo, and G. Barbaro. 2012. "Small-scale field experiment on wave forces on upright breakwaters." *J. Waterway, Port, Coastal, Ocean Eng.* 138 (2): 97–114. https://doi.org/10.1061/(ASCE)WW.1943-5460.0000111.

Boccotti, P., G. Barbaro, and L. Mannino. 1993. "A field experiment on the mechanics of irregular gravity waves." *J. Fluid Mech.* 252 (1): 173–186. https://doi.org/10.1017/S0022112093003714.

Byrd, R. H., J. C. Gilbert, and J. Nocedal. 2000. "A trust region method based on interior point techniques for nonlinear programming." *Math. Program.* 89 (1): 149–185. https://doi.org/10.1007/PL00011391.

Candes, E. J., J. Romberg, and T. Tao. 2006a. "Robust uncertainty principles: Exact signal reconstruction from highly incomplete frequency information." *IEEE Trans. Inf. Theory.* 52 (2): 489–509. https://doi.org/10.1109/TIT.2005.862083.

Candes, E. J., J. K. Romberg, and T. Tao. 2006b. "Stable signal recovery from incomplete and inaccurate measurements." *Commun. Pure Appl. Math.* 59 (8): 1207–1223. https://doi.org/10.1002/cpa.20124.

Candes, E. J., and T. Tao. 2005. "Decoding by linear programming." *IEEE Trans. Inf. Theory.* 51 (12): 4203–4215. https://doi.org/10.1109/TIT.2005.858979.

Candes, E. J., and T. Tao. 2006. "Near-optimal signal recovery from random projections: Universal encoding strategies?" *IEEE Trans. Inf. Theory.* 52 (12): 5406–5425. https://doi.org/10.1109/TIT.2006.885507.

Candes, E. J., and M. B. Wakin. 2008. "An introduction to compressive sampling." *IEEE Signal Process Mag.* 25 (2): 21–30. https://doi.org/10.1109/MSP.2007.914731.

Claerbout, J. F., and F. Muir. 1973. "Robust modeling with erratic data." *Geophys.* 38 (5): 826–844. https://doi.org/10.1190/1.1440378.

Comerford, L. A., M. Beer, and I. A. Kougioumtzoglou. 2014. "Compressive sensing based power spectrum estimation from incomplete records by utilizing an adaptive basis." *Proc., IEEE Symp. on Computational Intelligence for Engineering Solutions (CIES)*, 117–124. New York: Institute of Electrical and Electronics Engineers.

Comerford, L., H. A. Jensen, F. Mayorga, M. Beer, and I. A. Kougioumtzoglou. 2017. "Compressive sensing with an adaptive wavelet basis for structural system response and reliability analysis under missing data." *Comput. Struct.* 182: 26–40. https://doi.org/10.1016/j.compstruc.2016.11.012.

Comerford, L., I. A. Kougioumtzoglou, and M. Beer. 2015. "On quantifying the uncertainty of stochastic process power spectrum estimates subject to missing data." *Int. J. Sustainable Mater. Struct. Syst.* 2 (1/2): 185–206. https://doi.org/10.1504/IJSMSS.2015.078358.

Comerford, L., I. A. Kougioumtzoglou, and M. Beer. 2016. "Compressive sensing based stochastic process power spectrum estimation subject to missing data." *Probab. Eng. Mech.* 44: 66–76. https://doi.org/10.1016/j.probengmech.2015.09.015.

Constantin, A. 2012. "On the recovery of solitary wave profiles from pressure measurements." *J. Fluid Mech.* 699: 376–384. https://doi.org/10.1017/jfm.2012.114.

de Boor, C. 1978. *A practical guide to splines.* New York: Springer-Verlag.

Dean, R. G., and R. A. Dalrymple. 1991. *Water wave mechanics for engineers and scientists.* Singapore: World Scientific.

Deconinck, B., K. L. Oliveras, and V. Vasan. 2012. "Relating the bottom pressure and the surface elevation in the water wave problem." *J. Nonlinear Math. Phys.* 19 (sup1): 179–189. https://doi.org/10.1142/S1402925112400141.

Donoho, D. L. 2006. "Compressed sensing." *IEEE Trans. Inf. Theory.* 52 (4): 1289–1306. https://doi.org/10.1109/TIT.2006.871582.

Escher, J., and T. Schlurmann. 2008. "On the recovery of the free surface from the pressure within periodic traveling water waves." *J. Nonlinear Math. Phys.* 15 (sup2): 50–57. https://doi.org/10.2991/jnmp.2008.15.s2.4.

Haile, M., and A. Ghoshal. 2012. "Application of compressed sensing in full-field structural health monitoring." *Proc., SPIE 8346, Smart Sensor Phenomena, Technology, Networks, and Systems Integration*, 834618. https://www.spiedigitallibrary.org/conference-proceedings-of-spie/8346/834618/Application-of-compressed-sensing-in-full-field-structural-health-monitoring/10.1117/12.915429.short?SSO=1&tab=ArticleLink.

Harley, J. B., A. C. Schmidt, and J. M. F. Moura. 2012. "Accurate sparse recovery of guided wave characteristics for structural health monitoring." *Proc., 2012 IEEE International Ultrasonics Symp.*, 158–161. New York: Institute of Electrical and Electronics Engineers.

Hasselmann, K., et al. 1973. "Measurements of wind-wave growth and swell decay during the joint North Sea wave project (JONSWAP)." *Ergänzungsheft zur Deutschen Hydrographischen Zeitschrift.* A8: 1–95.

Huang, Y., J. L. Beck, S. Wu, and H. Li. 2014. "Robust Bayesian compressive sensing for signals in structural health monitoring." *Comput.-Aided Civ. Infrastruct. Eng.* 29 (3): 160–179. https://doi.org/10.1111/mice.12051.

Klis, R., and E. N. Chatzi. 2017. "Vibration monitoring via spectro-temporal compressive sensing for wireless sensor networks." *Struct. Infrastruct. Eng.* 13 (1): 195–209. https://doi.org/10.1080/15732479.2016.1198395.

Kougioumtzoglou, I. A., K. R. M. dos Santos, and L. Comerford. 2017. "Incomplete data based parameter identification of nonlinear and time-variant oscillators with fractional derivative elements." *Mech. Syst. Sig. Process.* 94: 279–296. https://doi.org/10.1016/j.ymssp.2017.03.004.

Kundu, P. K., I. M. Cohen, and D. R. Dowling. 2015. *Fluid mechanics.* London: Elsevier Science.

Kuo, Y.-Y., and J.-F. Chiu. 1995. "Transfer function between wave height and wave pressure for progressive waves: Reply to the comments of A. Baquerizo and M.A. Losada." *Coastal Eng.* 24 (3): 355–356. https://doi.org/10.1016/0378-3839(94)00039-Z.

Kuo, Y.-Y., and Y.-F. Chiu. 1994. "Transfer function between wave height and wave pressure for progressive waves." *Coastal Eng.* 23 (1): 81–93. https://doi.org/10.1016/0378-3839(94)90016-7.

Laface, V., I. A. Kougioumtzoglou, G. Malara, and F. Arena. 2017. "Efficient processing of water wave records via compressive sensing and joint time-frequency analysis via harmonic wavelets." *Appl. Ocean Res.* 69: 1–9. https://doi.org/10.1016/j.apor.2017.09.011.

Lee, H. S., and S. H. Kwon. 2003. "Wave profile measurement by wavelet transform." *Ocean Eng.* 30 (18): 2313–2328. https://doi.org/10.1016/S0029-8018(03)00114-8.

Levine, R. M., J. E. Michaels, and S. J. Lee. 2012. "Guided wave localization of damage via sparse reconstruction." *AIP Conf. Proc.* 1430 (1): 647–654.

Mascareñas, D., A. Cattaneo, J. Theiler, and C. Farrar. 2013. "Compressed sensing techniques for detecting damage in structures." *Struct. Health Monit.* 12 (4): 325–338. https://doi.org/10.1177/1475921713486164.

Newland, D. E. 1994. "Wavelet analysis of vibration: Part 1—Theory." *J. Vib. Acoust.* 116 (4): 409–416. https://doi.org/10.1115/1.2930443.

Nyquist, H. 1928. "Certain topics in telegraph transmission theory." *Trans. Am. Inst. Electr. Eng.* 47 (2): 617–644. https://doi.org/10.1109/T-AIEE.1928.5055024.

O'Connor, S. M., J. P. Lynch, and A. C. Gilbert. 2013. "Implementation of a compressive sampling scheme for wireless sensors to achieve energy efficiency in a structural health monitoring system." In *Proc., SPIE 8694, Nondestructive Characterization for Composite Materials, Aerospace Engineering, Civil Infrastructure, and Homeland Security*, 86941L-86941L-86911. Bellingham, WA: SPIE. https://www.spiedigitallibrary.org/conference-proceedings-of-spie/8694/1/Implementation-of-a-compressive-sampling-scheme-for-wireless-sensors-to/10.1117/12.2010128.short.

Oliveras, K. L., V. Vasan, B. Deconinck, and D. Henderson. 2012. "Recovering the water-wave profile from pressure measurements." *SIAM J. Appl. Math.* 72 (3): 897–918. https://doi.org/10.1137/110853285.

Perelli, A., L. De Marchi, L. Flamigni, A. Marzani, and G. Masetti. 2015. "Best basis compressive sensing of guided waves in structural health monitoring." *Digital Signal Process.* 42: 35–42. https://doi.org/10.1016/j.dsp.2015.04.001.

Phillips, O. M., D. Gu, and M. Donelan. 1993a. "Expected structure of extreme waves in a Gaussian sea. Part I: Theory and SWADE buoy measurements." *J. Phys. Oceanogr.* 23 (5): 992–1000. https://doi.org/10.1175/1520-0485(1993)023<0992:ESOEWI>2.0.CO;2.

Phillips, O. M., D. Gu, and E. J. Walsh. 1993b. "On the expected structure of extreme waves in a Gaussian sea. Part II: SWADE scanning radar altimeter measurements." *J. Phys. Oceanogr.* 23 (10): 2297–2309. https://doi.org/10.1175/1520-0485(1993)023<2297:OTESOE>2.0.CO;2.

Romolo, A., and F. Arena. 2013. "Three-dimensional non-linear standing wave groups: Formal derivation and experimental verification." *Int. J. Non Linear Mech.* 57: 220–239. https://doi.org/10.1016/j.ijnonlinmec.2013.08.005.

Romolo, A., F. Arena, and V. Laface. 2014. "A generalized approach to the mechanics of three-dimensional nonlinear ocean waves." *Probab. Eng. Mech.* 35: 96–107. https://doi.org/10.1016/j.probengmech.2013.10.009.

Shannon, C. 1949. "Comunication in the presence of noise." *Proc. Inst. Radio Eng.* 37 (1): 10–21.

Tau Siesakul, B., K. Gkoktsi, and A. Giaralis. 2015. "Compressive power spectrum sensing for vibration-based output-only system identification of structural systems in the presence of noise." In *Proc., SPIE Sensing Technology+Applications, International Society for Optics and Photonics*, 94840K. Bellingham, WA: SPIE. https://www.spiedigitallibrary.org/conference-proceedings-of-spie/9484/94840K/Compressive-power-spectrum-sensing-for-vibration-based-output-only-system/10.1117/12.2177162.short.

Tsai, C.-H., M.-C. Huang, F.-J. Young, Y.-C. Lin, and H.-W. Li. 2005. "On the recovery of surface wave by pressure transfer function." *Ocean Eng.* 32 (10): 1247–1259. https://doi.org/10.1016/j.oceaneng.2004.10.020.

Tsai, J.-C., and C.-H. Tsai. 2009. "Wave measurements by pressure transducers using artificial neural networks." *Ocean Eng.* 36 (15–16): 1149–1157. https://doi.org/10.1016/j.oceaneng.2009.08.007.

Viriyakijja, K., and C. Chinnarasri. 2015. "Wave flume measurement using image analysis." *Aquat. Procedia.* 4: 522–531. https://doi.org/10.1016/j.aqpro.2015.02.068.

Waltz, R. A., J. L. Morales, J. Nocedal, and D. Orban. 2006. "An interior algorithm for nonlinear optimization that combines line search and trust region steps." *Math. Program.* 107 (3): 391–408. https://doi.org/10.1007/s10107-004-0560-5.

Wang, Y., and H. Hao. 2015. "Damage identification scheme based on compressive sensing." *J. Comput. Civ. Eng.* 29 (2): 04014037. https://doi.org/10.1061/(ASCE)CP.1943-5487.0000324.

Yang, Y., and S. Nagarajaiah. 2015. "Output-only modal identification by compressed sensing: Non-uniform low-rate random sampling." *Mech. Syst. Sig. Process.* 56–57: 15–34. https://doi.org/10.1016/j.ymssp.2014.10.015.

Zhang, Y., L. Comerford, M. Beer, and I. Kougioumtzoglou. 2015. "Compressive sensing for power spectrum estimation of multi-dimensional processes under missing data." In *Proc., 2015 Int. Conf. on Systems, Signals and Image Processing (IWSSIP)*, 162–165. London: IEEE.

Zhang, Y., L. Comerford, I. Kougioumtzoglou, and M. Beer. 2018. "Lp-norm minimization for stochastic process power spectrum estimation subject to incomple data." *Mech. Syst. Sig. Process.* 101: 361–376. https://doi.org/10.1016/j.ymssp.2017.08.017.

Zou, Z., Y. Bao, H. Li, B. F. Spencer, and J. Ou. 2015. "Embedding compressive sensing-based data loss recovery algorithm into wireless smart sensors for structural health monitoring." *IEEE Sens. J.* 15 (2): 797–808.